

Thermopower in an anisotropic two-dimensional Weyl semimetal

Ipsita Mandal¹ and Kush Saha²

¹*Laboratory of Atomic And Solid State Physics, Cornell University, Ithaca, NY 14853, USA*

²*National Institute of Science Education and Research Bhubaneswar, Jatni, Khurda 752050, Odisha, India*

(Dated: December 15, 2024)

We investigate the generation of an electric current from a temperature gradient in a two-dimensional Weyl semimetal with anisotropy, both in the presence and absence of a quantizing magnetic field. We show that the anisotropy leads to doping dependences of thermopower and thermal conductivities which are different from those in isotropic Dirac materials. Additionally, we find that a quantizing magnetic field in such systems leads to an interesting magnetic field dependence of the longitudinal thermopower, resulting in unsaturated thermoelectric coefficients. Thus the results presented here will serve as a guide in achieving high thermopower and thermoelectric figure-of-merit in graphene-based materials, as well as organic conductors such as α -BEDT-TTF₂I₃.

I. INTRODUCTION

Since the discovery of Dirac materials in both two and three dimensions, there has been an upsurge in the study of thermopower in these systems, both in the presence and absence of a quantizing magnetic field.^{1–8} This is because the thermopower is a sensitive and powerful tool to probe transport properties, involving different scattering mechanisms in materials. Two-dimensional (2D) graphene and related 2D Dirac materials exhibit anomalous and universal thermoelectric properties due to the Weyl/Dirac dispersion of the emergent quasiparticles.^{5,9} Similarly, 3D Weyl systems exhibit anomalous thermal properties due to the Berry curvature.^{10–16} Moreover, the 3D Dirac and Weyl materials give rise to unsaturated thermopower, which in turn leads to large thermoelectric figure-of-merit in the presence of a quantizing magnetic field.¹⁷

Despite much work on the transport properties in Dirac/Weyl materials,^{18–29} the thermoelectric properties in relatively new 2D anisotropic Dirac materials such as VO₂/TiO₃,^{30–32} organic salts,^{33,34} and deformed graphene,^{35–38} having a quadratic dispersion in one direction and a linear dispersion along the orthogonal direction, have not been explored so far in details. This is in part because there are lack of natural materials with such anisotropic dispersion and in part because the anisotropy leads to complexities in finding the analytical expressions for relevant thermoelectric coefficients involving different scattering mechanism, as compared to the in-plane and out-of-plane anisotropy in double-Weyl materials.¹³ Due to the anisotropic dispersion, these 2D Dirac materials exhibit unconventional electric and magnetic properties as opposed to the isotropic Weyl/Dirac systems.^{39,40} Since transport coefficients such as thermal conductivity and thermoelectric coefficients are determined by the band structure and scattering mechanism, it is natural to ask how this anisotropy can be leveraged in the thermal properties of these 2D systems, both in the presence and absence of quantized magnetic field. Specifically, does this anisotropy give rise to interesting field, temperature and doping dependence of the thermoelectric coefficients?

To address these, we study the thermal transport in

such an anisotropic 2D Dirac/Weyl system, both in absence and in presence of an external magnetic field. We show that the thermopower in the absence of a magnetic field exhibits a complex dependence on the chemical potential and temperature, in contrast to its isotropic counterpart.^{3,15} We also find that the presence of an external magnetic field leads to interesting field-dependent thermal properties, leading to unsaturated thermopower. This field dependence differs notably not only from its isotropic counterpart, but also from the 3D Dirac/Weyl systems.¹⁷ This is attributed to the fact that the field dependence of the Landau spectrum ($\epsilon_n \sim (nH)^{2/3}$, where n is the Landau level and H is the applied magnetic field³⁹) for such anisotropic Dirac/Weyl systems differs from that ($\epsilon_n \sim \sqrt{nH}$) of the 2D and 3D isotropic Dirac/Weyl systems. We note that a similar anisotropic situation arises in a 3D double-Weyl material,¹³ where anisotropy is present in one of the three orthogonal directions. However, the result varies from the present case due to different density of states (DOS) in two different physical dimensions. Specifically, the DOS of a 3D anisotropic double-Weyl dispersion turns out to be $\rho(\epsilon) \sim |\epsilon|$, which simplifies the analytical expressions for the thermoelectric coefficients.¹³ In contrast, the DOS of a 2D anisotropic Dirac dispersion goes as $\rho(\epsilon) \sim \sqrt{|\epsilon|}$, which in turn leads to complex structures of the thermoelectric equations, hence complex chemical potential and magnetic field-dependent thermopower.

The rest of the paper is organized as follows. In Sec. II, we introduce anisotropic 2D Dirac/Weyl model Hamiltonian and define the thermoelectric coefficients. This is followed by Sec. III, where we provide analytical expressions for thermoelectric coefficients in zero magnetic field. We then compare our results with the case of isotropic Dirac dispersion. In Sec. IV–V, we present the results for diffusive transport and electron-electron interaction, respectively. We then extend these results for finite field in Sec. VI and discuss the unsaturated thermopower. Finally, we conclude with a discussion on the possible future directions in Sec. VII.

II. MODEL AND FORMALISM

We consider a model of 2D anisotropic Weyl fermion (AWF), with the Hamiltonian³⁰⁻³²

$$H_{\text{AWF}} = \frac{\hbar^2 k_x^2}{2m} \sigma_x + \hbar v k_y \sigma_y, \quad (1)$$

where σ_i 's are Pauli matrices, (k_x, k_y) are the momenta in the x and y directions, respectively, m is the effective mass along the x -axis, and v is the effective velocity along the y -axis. We will use $a = \frac{\hbar^2}{2m}$ and $b = \hbar v$ in the equations for simplifying the expressions. With these notations, the spectrum of Eq. (1) is obtained to be $\varepsilon_{\mathbf{k}}^{\pm} = \pm \sqrt{a_0^2 k_x^4 + b_0^2 k_y^2}$. This anisotropic nature of the spectrum is expected to manifest in the thermoelectric properties of the system.

The response matrix, which relates the resulting generalized currents to the driving forces, can be expressed in terms of some kinetic coefficients. We will use the relations obtained from the Boltzmann formalism, such that the response matrix takes the form:⁴¹

$$\begin{pmatrix} \mathbf{J}_{\alpha} \\ \mathbf{J}_{\alpha}^Q \end{pmatrix} = \begin{pmatrix} L_{\alpha\beta}^{11} & L_{\alpha\beta}^{12} \\ L_{\alpha\beta}^{21} & L_{\alpha\beta}^{22} \end{pmatrix} \begin{pmatrix} \mathbf{E}_{\beta} \\ -\nabla_{\beta} T \end{pmatrix}, \quad (2)$$

where $(\alpha, \beta) \in (x, y)$, \mathbf{J}^Q is the heat current and \mathbf{J} is the electrical current at temperature T , in presence of an electric field \mathbf{E} . The expressions for the longitudinal thermoelectric coefficients are given by:⁴¹

$$\begin{aligned} L_{\alpha\alpha}^{11} &= \sigma_{\alpha\alpha} = \mathcal{L}_{\alpha}^0, & L_{\alpha\alpha}^{21} &= T L_{\alpha\alpha}^{12} = \frac{-\mathcal{L}_{\alpha}^1}{e}, \\ L_{\alpha\alpha}^{22} &= \frac{\mathcal{L}_{\alpha}^2}{e^2 T}, \end{aligned} \quad (3)$$

with

$$\begin{aligned} \mathcal{L}_{\alpha}^n &= -e^2 \sum_{s=\pm} \int \frac{d^2 \mathbf{k}}{(2\pi)^2} \tau(\varepsilon_{\mathbf{k}}^s) \frac{\partial f(\varepsilon_{\mathbf{k}}^s)}{\partial \varepsilon_{\mathbf{k}}^s} \left(\frac{1}{\hbar} \frac{\partial \varepsilon_{\mathbf{k}}^s}{\partial k_{\alpha}} \right)^2 (\varepsilon_{\mathbf{k}}^s - \mu)^n, \end{aligned} \quad (4)$$

where $s = \pm$ is the band index, e is the electric charge, μ is the chemical potential and $f(\varepsilon) = \frac{1}{1+e^{\beta(\varepsilon-\mu)}}$ is the Fermi-Dirac distribution at inverse temperature $\beta = \frac{1}{k_B T}$ (k_B is the Boltzmann constant). The thermal conductivity and the Seebeck coefficient (thermopower) can

now be defined as:

$$\kappa_{\alpha\beta} = L_{\alpha\beta}^{22} - L_{\alpha\gamma}^{21} (L_{\gamma\rho}^{11})^{-1} L_{\rho\beta}^{12}, \quad \text{and} \quad S_{\alpha} = \frac{L_{\alpha\alpha}^{12}}{L_{\alpha\alpha}^{11}}, \quad (5)$$

respectively. The Seebeck coefficient describes the voltage generation due to a temperature gradient.

For the anisotropic dispersion in Eq. (1), we follow the methods outlined in Ref. 42. With the parametrization $k_x = \text{sign}[\cos \theta] \left(\frac{r |\cos \theta|}{a} \right)^{1/2}$ and $k_y = \frac{r \sin \theta}{b}$ with $r \geq 0$, the energy eigenvalues take the simple form $\varepsilon_{\mathbf{k}}^{\pm} = \pm r$. The Jacobian of this transformation is given by:

$$\begin{aligned} \mathcal{J}(r, \theta) &= \left| \frac{\partial k_x}{\partial r} \frac{\partial k_y}{\partial \theta} \right| = \left| \frac{1}{2} \left(\frac{|\cos \theta|}{a r} \right)^{1/2} - \frac{\sin \theta}{2} \left(\frac{r}{a |\cos \theta|} \right)^{1/2} \right| \\ &= \sqrt{\frac{r}{4 a b^2 |\cos \theta|}}. \end{aligned} \quad (6)$$

Let us apply this convenient parametrization for calculating the DOS at energy $\varepsilon > 0$, which is given by:

$$\begin{aligned} \rho(\varepsilon) &= \int \frac{d^2 \mathbf{k}}{(2\pi)^2} \delta(\varepsilon - \varepsilon_{\mathbf{k}}^+) \\ &= \int_0^{\infty} dr \int_0^{2\pi} \frac{d\theta}{(2\pi)^2} \mathcal{J}(r, \theta) \delta(\varepsilon - r) \\ &= \int_0^{2\pi} \frac{d\theta}{(2\pi)^2} \sqrt{\frac{\varepsilon}{4 a b^2 |\cos \theta|}} = \frac{10.4882}{8\pi^2} \sqrt{\frac{\varepsilon}{a b^2}}. \end{aligned} \quad (7)$$

Clearly, the DOS of the AWF differs from its isotropic counterpart, i.e., graphene, where $\rho(\varepsilon) \sim |\varepsilon|$ (see Appendix. A). Thus it is expected to have different thermopower and thermal conductivities, depending on the scattering mechanisms. However, it is not obvious how strongly this anisotropy will be manifested in the thermoelectric coefficients as functions of μ and T . In the following sections, we therefore compute the thermoelectric coefficients (i) for the free Hamiltonian, (ii) in the presence of short-range disorder, and (iii) in the presence of charge impurities. We then compare the results with those obtained for graphene. We also compare it with the isotropic and anisotropic 3D Dirac materials, wherever deemed necessary. Finally, we consider the case where an external magnetic field is applied, in order to determine the power-law dependence of the thermoelectric coefficients on the applied field strength.

III. THERMOELECTRIC RESPONSE FOR THE FREE HAMILTONIAN

Using the semiclassical approach for calculating the dc conductivity by assuming an energy and momentum independent scattering time τ , we get:

$$\begin{aligned}\sigma_{xx}^{\text{dc}} &= \mathcal{L}_x^0 = \frac{e^2 \tau \sqrt{a} \beta}{8 \pi^2 \hbar^2 b} \int_0^\infty dr \int_0^{2\pi} d\theta r^{3/2} |\cos \theta|^{5/2} \left[\text{sech}^2 \left(\frac{\beta(r-\mu)}{2} \right) + \text{sech}^2 \left(\frac{\beta(r+\mu)}{2} \right) \right] \\ &= -\frac{2.16 e^2 \tau \sqrt{a}}{2 \hbar^2 b (\pi \beta)^{3/2}} \left[\text{Li}_{3/2}(-e^{\beta \mu}) + \text{Li}_{3/2}(-e^{-\beta \mu}) \right],\end{aligned}\quad (8)$$

$$\begin{aligned}\sigma_{yy}^{\text{dc}} &= \mathcal{L}_y^0 = \frac{e^2 \tau b \beta}{32 \pi^2 \hbar^2 \sqrt{a}} \int_0^\infty dr \int_0^{2\pi} d\theta \sqrt{r |\sec \theta|} \sin^2 \theta \left[\text{sech}^2 \left(\frac{\beta(r-\mu)}{2} \right) + \text{sech}^2 \left(\frac{\beta(r+\mu)}{2} \right) \right] \\ &= -\frac{3.5 e^2 \tau b}{8 \pi^{3/2} \hbar^2 \sqrt{a} \beta} \left[\text{Li}_{1/2}(-e^{\beta \mu}) + \text{Li}_{1/2}(-e^{-\beta \mu}) \right],\end{aligned}\quad (9)$$

where $\text{Li}_s(z)$ denotes the polylogarithm function. For $\mu/(k_B T) \gg 1$, we obtain:

$$\sigma_{xx}^{\text{dc}} = \frac{2.88 e^2 \tau \sqrt{a}}{2 \pi^2 \hbar^2 b} \left(\mu^{3/2} + \frac{\pi^2}{8 \sqrt{\mu}} (k_B T)^2 \right), \quad (10)$$

$$\sigma_{yy}^{\text{dc}} = \frac{7 e^2 \tau b}{8 \pi^2 \hbar^2 \sqrt{a}} \left(\sqrt{\mu} - \frac{\pi^2}{24 \mu^{3/2}} (k_B T)^2 \right). \quad (11)$$

Evidently, the low-temperature longitudinal dc conductivities are direction-dependent, and have different doping dependence as well. This is because the group velocity $v_{\mathbf{k}} = \left(\frac{1}{\hbar} \frac{\partial \varepsilon_{\mathbf{k}}}{\partial k_\alpha} \right)$ in Eq. (4) differs in the x and y directions as $v_x \sim k_x \sigma_x$, and $v_y \sim \sigma_y$. This is in contrast to the case of isotropic Dirac Hamiltonian such as

graphene, where $v_x \sim \sigma_x$ and $v_y \sim \sigma_y$. Consequently, we obtain $\sigma_{xx} = \sigma_{yy} \sim \mu$, as derived in Appendix A. Thus, the anisotropic band spectrum or in other words, the DOS of the system plays important role in revealing anisotropic dc conductivities. We note that for 3D double-Weyl Dirac semimetals with anisotropy in $x-y$ plane (dispersion $\varepsilon_{\mathbf{k}} = \sqrt{\frac{\hbar^2(k_x^2 + k_y^2)^2}{2m}} + v^2 k_z^2$), the DOS turns out to be $\rho(\varepsilon) \sim |\varepsilon|$ similar to 2D graphene. Thus, the z -component of the dc conductivities shows similar dependence as graphene, however the x and y -components depend quadratically on both chemical potential and temperature¹³ but differs from the present model.

The thermoelectric coefficients are obtained in a similar fashion, as shown below:

$$\begin{aligned}L_{xx}^{21} &= \frac{e \tau \sqrt{a} \beta}{8 \pi^2 \hbar^2 b} \int_0^\infty dr \int_0^{2\pi} d\theta r^{3/2} |\cos \theta|^{5/2} \left[\mu \left\{ \text{sech}^2 \left(\frac{\beta(r+\mu)}{2} \right) + \text{sech}^2 \left(\frac{\beta(r-\mu)}{2} \right) \right\} \right. \\ &\quad \left. + r \left\{ \text{sech}^2 \left(\frac{\beta(r+\mu)}{2} \right) - \text{sech}^2 \left(\frac{\beta(r-\mu)}{2} \right) \right\} \right] \\ &= -\frac{2.16 e \tau \sqrt{a}}{2 \hbar^2 b (\pi \beta)^{3/2}} \left[\mu \left\{ \text{Li}_{3/2}(-e^{-\beta \mu}) + \text{Li}_{3/2}(-e^{\beta \mu}) \right\} + \frac{5}{2 \beta} \left\{ \text{Li}_{5/2}(-e^{-\beta \mu}) - \text{Li}_{5/2}(-e^{\beta \mu}) \right\} \right],\end{aligned}\quad (12)$$

$$\begin{aligned}L_{yy}^{21} &= \frac{e \tau b \beta}{32 \pi^2 \hbar^2 \sqrt{a}} \int_0^\infty dr \int_0^{2\pi} d\theta \sqrt{r |\sec \theta|} \sin^2 \theta \left[\mu \left\{ \text{sech}^2 \left(\frac{\beta(r+\mu)}{2} \right) + \text{sech}^2 \left(\frac{\beta(r-\mu)}{2} \right) \right\} \right. \\ &\quad \left. + r \left\{ \text{sech}^2 \left(\frac{\beta(r+\mu)}{2} \right) - \text{sech}^2 \left(\frac{\beta(r-\mu)}{2} \right) \right\} \right] \\ &= -\frac{3.5 e \tau b}{8 \pi^{3/2} \hbar^2 \sqrt{a} \beta} \left[\mu \left\{ \text{Li}_{1/2}(-e^{-\beta \mu}) + \text{Li}_{1/2}(-e^{\beta \mu}) \right\} + \frac{3}{2 \beta} \left\{ \text{Li}_{3/2}(-e^{-\beta \mu}) - \text{Li}_{3/2}(-e^{\beta \mu}) \right\} \right],\end{aligned}\quad (13)$$

At low temperatures, i.e., $\mu/(k_B T) \gg 1$, we obtain:

$$\begin{aligned}L_{xx}^{21} &= -\frac{2.88 e \tau \sqrt{a}}{2 \pi^2 \hbar^2 b} \left(\frac{\pi^2 \mu^{1/2}}{2} (k_B T)^2 \right), \\ L_{yy}^{21} &= -\frac{7 e \tau b}{8 \pi^2 \hbar^2 \sqrt{a}} \left(\frac{\pi^2}{6 \mu^{1/2}} (k_B T)^2 \right).\end{aligned}\quad (14)$$

As before, the low-temperature behavior of the off-diagonal longitudinal thermal coefficients have an interesting direction dependence on the chemical potential. In contrast, for graphene $L_{xx} = L_{yy} = \pi (k_B T)^2$ are independent of chemical potential. Although the individual

coefficients in the AWF differ from those in graphene, the Mott relation still prevails at low temperature as follows:

$$\begin{aligned} S_{xx} &= \frac{L_{xx}^{21}}{T \sigma_{xx}^{\text{dc}}} \simeq -\frac{k_B T}{2 e \mu}, \\ S_{yy} &= \frac{L_{yy}^{21}}{T \sigma_{xx}^{\text{dc}}} \simeq -\frac{k_B T}{6 e \mu}. \end{aligned} \quad (15)$$

Indeed, at low-temperature and for energy-independent scattering, there is no deviation of thermopower from the usual Mott relation. However, different energy-dependent scattering mechanisms may lead to deviation³ from the linear temperature dependent Mott relation as will be evident shortly.

To investigate the electronic contribution to the thermal conductivity κ , we next compute:

$$\begin{aligned} L_{xx}^{22} &= \frac{\mathcal{L}_x^2}{e^2 T} \\ &= \frac{\tau \sqrt{a} \beta}{8 \pi^2 \hbar^2 b T} \int_0^\infty dr \int_0^{2\pi} d\theta r^{3/2} |\cos \theta|^{5/2} \left[\text{sech}^2 \left(\frac{\beta(r+\mu)}{2} \right) (r+\mu)^2 + \text{sech}^2 \left(\frac{\beta(r-\mu)}{2} \right) (r-\mu)^2 \right] \\ &= -\frac{2.16 \tau \sqrt{a}}{2 \hbar^2 b (\pi \beta)^{3/2} T} \left[\mu^2 \left\{ \text{Li}_{3/2}(-e^{-\beta \mu}) + \text{Li}_{3/2}(-e^{\beta \mu}) \right\} + \frac{5 \mu}{\beta} \left\{ \text{Li}_{5/2}(-e^{-\beta \mu}) - \text{Li}_{5/2}(-e^{\beta \mu}) \right\} \right. \\ &\quad \left. + \frac{35}{4 \beta^2} \left\{ \text{Li}_{7/2}(-e^{-\beta \mu}) + \text{Li}_{7/2}(-e^{\beta \mu}) \right\} \right], \end{aligned} \quad (16)$$

$$\begin{aligned} L_{yy}^{22} &= \frac{\mathcal{L}_y^2}{e^2 T} \\ &= \frac{\tau b \beta}{32 \pi^2 \hbar^2 \sqrt{a} T} \int_0^\infty dr \int_0^{2\pi} d\theta \sqrt{r} |\sec \theta| \sin^2 \theta \left[\text{sech}^2 \left(\frac{\beta(r+\mu)}{2} \right) (r+\mu)^2 + \text{sech}^2 \left(\frac{\beta(r-\mu)}{2} \right) (r-\mu)^2 \right] \\ &= -\frac{3.5 e^2 \tau b}{8 \pi^{3/2} \hbar^2 \sqrt{a} \beta T} \left[\mu^2 \left\{ \text{Li}_{1/2}(-e^{-\beta \mu}) + \text{Li}_{1/2}(-e^{\beta \mu}) \right\} + \frac{3 \mu}{\beta} \left\{ \text{Li}_{3/2}(-e^{-\beta \mu}) - \text{Li}_{3/2}(-e^{\beta \mu}) \right\} \right. \\ &\quad \left. + \frac{15}{4 \beta^2} \left\{ \text{Li}_{5/2}(-e^{-\beta \mu}) + \text{Li}_{5/2}(-e^{\beta \mu}) \right\} \right]. \end{aligned} \quad (17)$$

At low temperatures ($\mu/(k_B T) \gg 1$), we obtain:

$$\begin{aligned} L_{xx}^{22} &= \frac{2.88 \tau \sqrt{a}}{2 \pi^2 \hbar^2 b T} \\ &\quad \times \left(\frac{\pi^2 \mu^{3/2}}{3} (k_B T)^2 + \frac{7 \pi^4}{40 \mu^{1/2}} (k_B T)^4 \right), \\ L_{yy}^{22} &= \frac{7 \tau b}{8 \pi^2 \hbar^2 \sqrt{a} T} \\ &\quad \left(\frac{\pi^2 \mu^{1/2}}{3} (k_B T)^2 - \frac{7 \pi^4}{120 \mu^{3/2}} (k_B T)^4 \right). \end{aligned} \quad (18)$$

Together with Eq. (18) and (11), we recover the Wiedemann-Franz law, $L_{\alpha\alpha}^{22} = \frac{\pi^2 k_B^2 T}{3 e^2} \sigma_{\alpha\alpha}^{\text{dc}}$, up to lead-

ing order in $k_B T$. Finally, using Eq. (5), we get:

$$\begin{aligned} \kappa_{xx} &= L_{xx}^{22} - \frac{(L_{xx}^{21})^2}{T \sigma_{xx}^{\text{dc}}} \\ &= \frac{2.88 \tau \sqrt{a}}{2 \pi^2 \hbar^2 b T} \left[\frac{\pi^2 \mu^{3/2} (k_B T)^2}{3} - \frac{3 \pi^4 (k_B T)^3}{40 \mu^{1/2}} \right], \\ \kappa_{yy} &= L_{yy}^{22} - \frac{(L_{yy}^{21})^2}{T \sigma_{yy}^{\text{dc}}} \\ &= \frac{7 \tau b}{8 \pi^2 \hbar^2 \sqrt{a} T} \left[\frac{\pi^2 \mu^{1/2} (k_B T)^2}{3} - \frac{31 \pi^4 (k_B T)^3}{360 \mu^{3/2}} \right]. \end{aligned} \quad (19)$$

As expected, the thermal conductivities shows linear dependence on temperature for both x and y direction. However, their chemical potential dependences differ by μ as a result of anisotropic dispersion as discussed before. We note that we have neglected phonon contribution to the thermal conductivity for simplicity. For strong contribution from phonon may lead to violation of the Wiedemann-Franz law.

Let us also state our results in the opposite limit of

$\mu/(k_B T) \ll 1$. In this high temperature limit, we get:

$$\begin{aligned}\sigma_{xx}^{\text{dc}} &\simeq \frac{2.16 e^2 \tau \sqrt{a}}{2 \hbar^2 b (\pi \beta)^{3/2}} \left(1.5303 + \frac{0.3801 \mu^2}{k_B^2 T^2} \right), \\ \sigma_{yy}^{\text{dc}} &\simeq \frac{3.5 e^2 \tau b}{8 \pi^{3/2} \hbar^2 \sqrt{a} \beta} \left(1.2098 + \frac{0.1187 \mu^2}{k_B^2 T^2} \right), \\ L_{xx}^{21} &= -\frac{2.16 e^2 \tau \sqrt{a}}{2 \hbar^2 b (\pi \beta)^{3/2}} \times 2.3 \mu, \\ L_{yy}^{21} &= -\frac{3.5 e^2 \tau b}{8 \pi^{3/2} \hbar^2 \sqrt{a} \beta} \times 0.60 \mu, \\ L_{xx}^{22} &= \frac{2.16 e^2 \tau \sqrt{a} \beta^2}{2 T \hbar^2 b (\pi \beta)^{3/2}} \left(16.88 + 0.6 \frac{\mu^2}{k_B^2 T^2} \right), \\ L_{yy}^{22} &= \frac{3.5 e^2 \tau b \beta^2}{8 \pi^{3/2} \hbar^2 \sqrt{a} \beta} \left(6.54 - 0.15 \frac{\mu^2}{k_B^2 T^2} \right). \quad (20)\end{aligned}$$

It turns out that the prefactors of both Eq. (8) and Eq. (12) give rise to dominant leading order contribution at high temperatures. Thus both σ and L^{21} goes as $T^{3/2}$. Consequently, we obtain thermopower decaying with temperature. However, for isotropic Dirac dispersion the leading order of σ_{xx} turns out to be T , whereas $L^{21} \sim T^2$. This leads to temperature independent thermopower in graphene at high temperature.³

IV. DIFFUSIVE TRANSPORT DUE TO DISORDER

We now consider the case of short-range disorder, which is less realistic for Weyl/Dirac semimetals, because the relatively poor screening of charged impurities lead to longer-range potentials. Nevertheless, it is useful to investigate the predictions for the thermal properties in this case for the purposes of comparison. The short-range disorder potential has the following form:

$$V(\mathbf{r}) = V_0 \sum_i \delta(\mathbf{r} - \mathbf{r}_i), \quad (21)$$

where \mathbf{r}_i denotes position of impurity potential and V_0 denotes the strength of the impurity potential. The scattering time for such disorder potential is calculated to be³⁶

$$\tau_{\text{dis}} = \frac{\tau_0(\varepsilon)}{1 + 0.435 \cos \theta}, \quad (22)$$

where $\tau_0(\varepsilon) = \frac{\hbar}{\pi \gamma \rho(\varepsilon)}$, $\gamma = V_0^2 n_{\text{imp}}$, and n_{imp} is the impurity concentration. Considering this energy dependence of the scattering rate ($\tau \sim \frac{1}{\sqrt{\varepsilon}}$), the transport coefficients at low temperatures ($\mu/(k_B T) \gg 1$) are found to be:

$$\begin{aligned}\sigma_{xx}^{\text{dc}} &\simeq \frac{2.88 e^2 \tau \sqrt{a}}{2 \pi^2 \hbar^2 b} \mu, \quad \sigma_{yy}^{\text{dc}} \simeq \frac{7 e^2 \tau b}{8 \pi^2 \hbar^2 \sqrt{a}}, \\ L_{xx}^{21} &\simeq -\frac{2.88 e \tau \sqrt{a}}{2 \pi^2 \hbar^2 b} \frac{(\pi k_B T)^2}{3}, \quad L_{yy}^{21} \simeq -\frac{7 e \tau b}{8 \pi^2 \hbar^2 \sqrt{a}} \mu. \quad (23)\end{aligned}$$

Evidently, the thermopower S_{xx} follows the Mott relation, whereas S_{yy} turns out to be independent of temperature (up to leading order). In contrast, for short-range disorder, the thermopower in graphene is exponentially suppressed at low temperature since $\tau_{\text{dis}} \sim 1/\varepsilon$.³

V. TRANSPORT IN PRESENCE OF CHARGED IMPURITY SCATTERINGS

Presence of charged impurities in a material act as dopants, thus shifting the Fermi level away from the nodal points. The screened Coulomb potential generated by such impurities is given by:

$$V(q) = \frac{4 \pi e^2}{q + q_{TF}}, \quad (24)$$

where q_{TF} is the Thomas-Fermi wave-vector. The transport relaxation time within the Born approximation is given by:

$$\begin{aligned}\frac{1}{\tau(\varepsilon_{\mathbf{k}}^s)} &= \frac{2 \pi n_{\text{imp}}}{\hbar} \int \frac{d^2 \mathbf{k}'}{(2 \pi)^2} V^2(|\mathbf{k} - \mathbf{k}'|) F_{\mathbf{k} \mathbf{k}'} \delta(\varepsilon_{\mathbf{k}}^s - \varepsilon_{\mathbf{k}'}^s), \quad (25)\end{aligned}$$

where $F_{\mathbf{k} \mathbf{k}'} = \frac{1 - \cos^2 \phi_{\mathbf{k} \mathbf{k}'}}{2}$, $\phi_{\mathbf{k} \mathbf{k}'}$ is the angle between \mathbf{k} and \mathbf{k}' and n_{imp} is the impurity density. Using the parametrization introduced before, $\cos \phi_{\mathbf{k} \mathbf{k}'}$ takes the form:

$$\begin{aligned}\cos \phi_{\mathbf{k} \mathbf{k}'} &= \frac{s_0 \sqrt{\alpha} |\cos \theta| \sqrt{\alpha} |\cos \theta'| + \sqrt{r} r' \sin \theta \sin \theta'}{\sqrt{\alpha} |\cos \theta| + r \sin^2 \theta} \frac{\sqrt{\alpha} |\cos \theta'| + r' \sin^2 \theta'}{\sqrt{\alpha} |\cos \theta'| + r' \sin^2 \theta'} \quad (26)\end{aligned}$$

where $\alpha = b^2/a$, $s_0 = \text{sign}[\cos \theta] \text{sign}[\cos \theta']$, and $(r, r') \geq 0$. For definiteness, let us consider the case when $s = +$. Since $\varepsilon_{\mathbf{k}}^+ = r$ is independent of θ , we set $\theta = \frac{\pi}{2}$ without any loss of generality. This leads to

$$F_{\mathbf{k}, \mathbf{k}'} = \frac{\alpha |\cos(\theta')|}{2 (|\cos \theta'| + r' \sin^2 \theta')}. \quad (27)$$

Together with Eq. (27), (25) and (6), we obtain

$$\begin{aligned}\frac{1}{\tau(r)} &= \frac{4 \pi n_{\text{imp}} e^4 \alpha}{\hbar r^{3/2}} \int \frac{d\theta'}{\left((1 - \sin^2 \theta')^2 + \frac{\alpha |\cos \theta'|}{r} \right)} \\ &\quad \times \frac{\sqrt{\alpha} |\cos \theta'|}{\alpha |\cos \theta'| + r \sin^2 \theta'}, \quad (28)\end{aligned}$$

where we have considered $q_{TF} = 0$ for unscreened charge impurities. In this case, Eq. (28) can be further simplified in the various limits as follows (assuming $\alpha \sim 1$):

$$\frac{1}{\tau(r)} \simeq \frac{4 \pi e^4 n_{\text{imp}}}{\hbar} \begin{cases} \frac{8.0}{r} & \text{for } r \ll 1, \\ \frac{6.0476}{r^{5/3}} + \frac{16.509}{r^{7/3}} - \frac{10.6889}{r^3} & \text{for } r \gg 1, \end{cases} \quad (29)$$

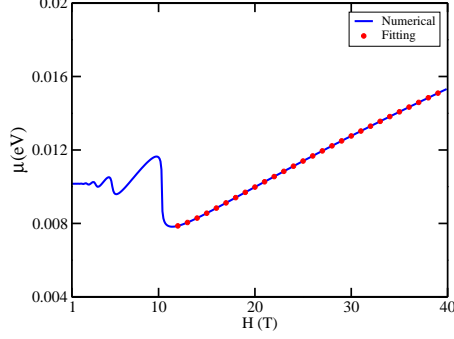


FIG. 1. Plot (blue solid line) of chemical potential as a function of magnetic field for fixed electron density $n_0 = 5 \times 10^{11} \text{ cm}^{-2}$ and temperature $T = 5 \text{ K}$. The strong field part of the red dotted line is the approximate analytical results in Eq. (36), where $b_0 = 0.0017$, $b_1 = 0.0006$, $b_2 = 0.0028$. Considering typical parameters of Dirac materials, we have used $v = 5 \times 10^5 \text{ m/s}$ and $m = 3.1 \times m_e$, where m_e is the electron mass. With this mass parameter (m), the cyclotron frequency $\omega_c \sim 50 \text{ GHz} - 2 \text{ THz}$ for the range of magnetic field presented in the plot.

The first limit is found from the leading order contribution of $2 \int_{-\pi/2+r}^{\pi/2-r} \frac{d\theta' \sqrt{|\cos \theta'|}}{\left(\frac{|\cos \theta'|}{r}\right)(|\cos \theta'|)}$, whereas the second limit is found from the leading order contribution of $4 \int_0^{\pi/2-(\frac{4}{r})^{1/3}} \frac{d\theta' \sqrt{|\cos \theta'|}}{(1-\sin \theta')^2 r \sin^2 \theta'}$.

We emphasize that the scattering from the unscreened Coulomb interaction in graphene is known to be $\tau \sim \varepsilon$ irrespective of the values of ε . In contrast, the anisotropy in Eq. (1) leads to a different expression for energy-dependent scattering for $\varepsilon \gg 1$. Considering the leading energy dependent term for $\tau \sim \varepsilon^{5/3}$, we find

$$\begin{aligned} \sigma_{xx}^{\text{dc}} &= \frac{2.88 e^2 \tau \sqrt{a}}{2 \pi^2 \hbar^2 b} \left(\mu^{19/6} + \frac{247 \mu^{7/6} \pi^2}{216} (k_B T)^2 \right), \\ \sigma_{yy}^{\text{dc}} &= \frac{7 e^2 \tau b}{8 \pi^2 \hbar^2 \sqrt{a}} \left(\mu^{13/6} + \frac{91 \mu^{1/6} \pi^2}{216} (k_B T)^2 \right), \\ L_{xx}^{21} &= -\frac{2.88 e \tau \sqrt{a}}{2 \pi^2 \hbar^2 b} \times \frac{19 \pi^2 \mu^{13/6} (k_B T)^2}{18}, \\ L_{yy}^{21} &= -\frac{7 e \tau b}{8 \pi^2 \hbar^2 \sqrt{a}} \times \frac{13 \pi^2 \mu^{7/6} (k_B T)^2}{18}. \end{aligned} \quad (30)$$

Thus we recover the Mott relation of $S_{\alpha\alpha} \sim T$. However, the dc conductivities have an interesting chemical potential dependence due to energy-dependent scatterings. This is in conjunction with the results obtained before.

VI. THERMOPOWER IN PRESENCE OF A MAGNETIC FIELD

Having obtained the zero magnetic field thermopower, we next turn to the finite field thermopower (Seebeck coefficient $S_{\alpha\alpha}(B)$). We mainly focus on the Seebeck coefficient along the x direction, following the heat current along x direction. It is already known that the Seebeck coefficient can be expressed as $S_{xx} = \frac{S}{e n_0}$, where S is the total entropy, and n_0 is the electron density. The total entropy can be expressed in terms of Fermi-Dirac distribution f function as:^{6,17}

$$S = k_B \sum_n [f_n \ln f_n + (1 - f_n) \ln (1 - f_n)], \quad (31)$$

where $f_n = f(\varepsilon_n - \mu)$, and ε_n denotes the Landau level energy.

For a magnetic field $\mathbf{H} = H \hat{\mathbf{z}}$, and using the Landau gauge $\mathbf{A} = (-H y, 0, 0)$, the Landau levels are obtained to be:³⁹

$$\begin{aligned} \varepsilon_n &= \pm 1.17325 (m v^2)^{1/3} [(n + 1/2) \hbar \omega_c]^{2/3}, \\ \omega_c &= \frac{e H}{m}. \end{aligned} \quad (32)$$

Here, ω_c is the effective cyclotron frequency and $n = 0, \pm 1, \pm 2, \dots$. With this, we find:

$$S_{xx} = \frac{k_B}{2 \pi n_0 e l_b^2} \sum_n \left[\ln(1 + e^{\tilde{x}_n}) - \frac{\tilde{x}_n e^{\tilde{x}_n}}{e^{\tilde{x}_n} + 1} \right], \quad (33)$$

where $\tilde{x}_n = \beta(\varepsilon_n - \mu)$, $l_b = \sqrt{\frac{\hbar}{e H}}$ is the magnetic length, and n_0 fixes the Fermi energy through

$$n_0 = 2 \times \frac{1}{2 \pi l_b^2} \sum_{n=0}^{\infty} f_n. \quad (34)$$

Here the factor of 2 accounts for the hole Landau levels. For a reasonably strong magnetic field ($\hbar \omega_c \gg \mu$), the system enters into a strong quantum limit and electrons occupy the lowest Landau level only. With this assumption, we can approximate Eq. (34) as:

$$n_0 \simeq \frac{1}{\pi l_b^2} \times \frac{1}{1 + e^{\beta(\varepsilon_0 - \mu)}}. \quad (35)$$

This leads to $\mu = \varepsilon_0 - \beta^{-1} \ln(\frac{1}{n_0 \pi l_b^2} - 1)$, which can be expressed in terms of explicit field dependence as

$$\mu = b_0 + b_1 H^{2/3} + b_2 \ln(b_3 H - 1), \quad (36)$$

where b_i 's can be readily obtained from the approximate analytical solution of μ . Interestingly, this approximate analytical result fits reasonably well with the numerical solution obtained from Eq. (35). Fig. (1) corroborates this. Notably, Eq. (36) differs from the case of 3D Dirac/Weyl systems (having $\mu \sim \frac{1}{H}$) and doped semiconductors (having $\mu \sim \frac{1}{H^2}$), as studied in Ref. 17. This

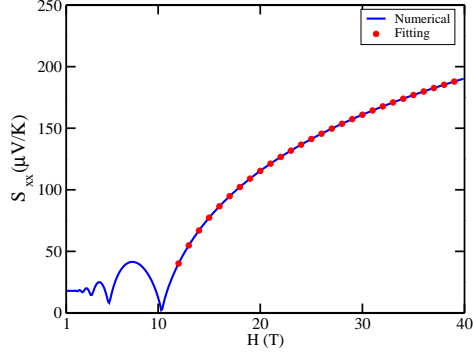


FIG. 2. Plot (blue solid line) of S_{xx} as a function of magnetic field for fixed electron density $n = 5 \times 10^{11} \text{ cm}^{-2}$ and temperature $T = 5 \text{ K}$. The red dotted line is the approximate analytical result with the function shown in Eq. (37). Values of the parameters v and m are the same as in Fig. (1).

difference again comes from different magnetic field dependence of the Landau spectrum. Notice that for weak enough magnetic field ($\hbar\omega_c \ll \mu$), the chemical potential mainly unaffected by the field. As we increase the field, we start to see quantum oscillations in the chemical potential, which in turn leads to oscillations in the thermopower, as will be evident shortly.

To find approximate high field dependence of the thermopower, we substitute Eq. (36) in Eq. (33) with $n = 0$. This gives

$$\begin{aligned} S_{xx} &= \frac{k_B}{e} \left[(\pi n_0 l_b^2) \ln(1 - \pi n_0 l_b^2) - \ln\left(\frac{1}{\pi n_0 l_b^2} - 1\right) \right] \\ &= \frac{k_B}{e} \left[\left(1 - \frac{H}{\alpha_0}\right) \ln\left(1 - \frac{\alpha_0}{H}\right) - \ln\left(\frac{\alpha_0}{H}\right) \right], \end{aligned} \quad (37)$$

where $\alpha_0 = \frac{n_0 \hbar}{2e}$. To verify this complex H -dependence, we numerically compute Eq. (33) along with the numerical solution of $\mu(H)$. In Fig. (2), we have plotted the behavior of S_{xx} as a function of H . Clearly, the approximate large field dependence of S_{xx} fits well (solid red dotted line) with the numerical solutions.

Note that, this field dependence differs from the behavior of doped semiconductors and from typical Dirac/Weyl systems,¹⁵ where $S_{xx} \sim H^2$. We would like to point out that the thermopower here turns out to be large compared to 2D semiconductors such as GaAs/Ga_{1-x}Al_xAs and Si-MOSFET.⁴³ This is indeed due to the Dirac nature of the quasiparticles with low Dirac velocity and low zeroth order Landau energy, as pointed out by several authors in the context of graphene.⁹⁷ Interestingly, the thermopower obtained for the present case has good agreement with the experimental results as found in α -BEDT-TTF₂I₃.[?]

To this end, we comment on the transverse thermoelectric coefficient S_{xy} , namely the magneto-thermoelectric Nernst-Ettinghausen effect. In the presence of a magnetic field, a voltage develops along the mutually perpendicular magnetic field $H(\parallel z)$ and temperature gradient $\nabla_x T$ due to the fact that the temperature-driven diffusing carriers experience a Lorentz force. This leads to the Nernst coefficient, which is defined as $S_{xy} = L_{xy}^{12}/L_{xy}^{11}$, where $L_{xy}^{11} = -\sum_n \int d\varepsilon f'(\varepsilon) \sigma_{xy}(\varepsilon)$ and $L_{xy}^{12} = -\sum_n \int d\varepsilon f'(\varepsilon)(\varepsilon - \mu) \sigma_{xy}(\varepsilon)$. It turns out that S_{xy} oscillates as a function of chemical potential. The maximum value of S_{xy} turns out to be $\frac{k_B}{e} \ln 2$, corroborating the universal behavior as pointed out by Girvin *et al.*[?] However, the peak position differs from graphene or typical semiconductors. We again attribute this difference to the difference in Landau spectrum, as discussed before.

VII. CONCLUSION

In this paper, we have studied the zero and finite magnetic field thermoelectric coefficients in an anisotropic 2D Weyl system, with the two anisotropic directions having linear and quadratic dispersions respectively. We have shown that this intrinsic anisotropy leads to an interesting doping and temperature dependence of the thermopower, compared to its isotropic counterpart. Our findings can be summarized as follows: (i) the low temperature dc conductivities have a different Fermi energy dependence as opposed to the case of graphene (having 2D isotropic Weyl dispersion); (ii) the high temperature thermopower decays with temperature in AWF, whereas it is independent of temperature in graphene; (iii) the relaxation rates due to diffusive and electron-electron interactions differ from the case of graphene, resulting in distinct expressions for the thermal and dc conductivities; (iv) the finite field thermopower has an interesting magnetic field dependence, resulting in unsaturated thermopower. We note that the results obtained here for a single node anisotropic Dirac/Weyl system can be used for multinode systems, provided that there is no internode scattering.

We conclude that the doping and temperature dependence of the transport measurements can be used to distinguish Dirac materials exhibiting anisotropy. In addition, the field dependent large thermopower can have potentials for thermoelectric devices to transform heat into electric power. In future work, it will be worthwhile to analyze the effects of Coulomb as well as short-ranged four-fermion interactions, and impurities, as has been done in the case of 2D^{44,45} and 3D⁴⁶⁻⁴⁸ isotropic semimetals with quadratic band touching points.

Appendix A: Thermoelectric response for the 2D Weyl semimetal

In this section, we compute the response matrix for the 2D isotropic Weyl semimetal, with the Hamiltonian

$$H_D = v (k_x \sigma_x + k_y \sigma_y). \quad (\text{A1})$$

Here we can use the usual polar coordinate parametrization $k_x = r \cos \theta$ and $k_y = r \sin \theta$ with $r \geq 0$, such that the energy eigenvalues are given by $\varepsilon_{\mathbf{k}}^{\pm} = \pm v r$. The Jacobian of this transformation is given by:

$$\mathcal{J}(r, \theta) = \begin{vmatrix} \frac{\partial k_x}{\partial r} & \frac{\partial k_x}{\partial \theta} \\ \frac{\partial k_y}{\partial r} & \frac{\partial k_y}{\partial \theta} \end{vmatrix} = r. \quad (\text{A2})$$

The density of states is $\rho(\varepsilon) = \frac{|\varepsilon|}{2\pi v^2}$.

We compute the dc conductivity by assuming an energy and momentum independent scattering time, such that:

$$\sigma_{xx}^{\text{dc}} = \sigma_{yy}^{\text{dc}} = \mathcal{L}_x^0 = \mathcal{L}_y^0 = \frac{\beta v^2 e^2 \tau}{8 \pi \hbar^2} \int_0^\infty dr r \left[\text{sech}^2 \left(\frac{\beta(r+\mu)}{2} \right) + \text{sech}^2 \left(\frac{\beta(r-\mu)}{2} \right) \right] = \frac{e^2 \tau \ln[2 + 2 \cosh(\beta \mu)]}{4 \pi \hbar^2 \beta}. \quad (\text{A3})$$

At low temperatures ($\mu/(k_B T) \gg 1$), we obtain $\sigma \sim \mu$.

The thermoelectric coefficients are given by:

$$\begin{aligned} L_{xx}^{21} = L_{yy}^{21} &= \frac{-\mathcal{L}_x^1}{e} = \frac{-\mathcal{L}_y^1}{e} \\ &= \frac{\beta v^2 e \tau}{8 \pi^2 \hbar^2} \int_0^\infty dr r \left[\mu \left\{ \text{sech}^2 \left(\frac{\beta(r+\mu)}{2} \right) + \text{sech}^2 \left(\frac{\beta(r-\mu)}{2} \right) \right\} + r \left\{ \text{sech}^2 \left(\frac{\beta(r+\mu)}{2} \right) - \text{sech}^2 \left(\frac{\beta(r-\mu)}{2} \right) \right\} \right] \\ &= -\frac{v e \tau}{(2 \beta \pi \hbar)^2} \left[\beta \mu \ln \{2 + 2 \cosh(\beta \mu)\} + 2 \text{Li}_2(-e^{\beta \mu}) - 2 \text{Li}_2(-e^{-\beta \mu}) \right], \end{aligned} \quad (\text{A4})$$

$$\begin{aligned} L_{xx}^{22} = L_{yy}^{22} &= \frac{\mathcal{L}_x^2}{e^2 T} = \frac{\mathcal{L}_y^2}{e^2 T} \\ &= \frac{\beta v^2 \tau}{8 \pi \hbar^2 T} \int_0^\infty dr r \left[\text{sech}^2 \left(\frac{\beta(r+\mu)}{2} \right) (r \varepsilon_0 + \mu)^2 + \text{sech}^2 \left(\frac{\beta(r-\mu)}{2} \right) (r - \mu)^2 \right] \\ &= \frac{v \tau}{4 \pi \hbar^2 T} \left[\frac{4 \mu \{ \text{Li}_2(-e^{-\beta \mu}) - \text{Li}_2(-e^{\beta \mu}) \}}{\beta} + \frac{6 \text{Li}_3(-e^{\beta \mu}) + 6 \text{Li}_3(-e^{-\beta \mu})}{\beta^2} - \mu^2 \ln \{2 + 2 \cosh(\beta \mu)\} \right]. \end{aligned} \quad (\text{A5})$$

At low temperatures, we get:

$$L_{xx}^{21} = L_{yy}^{21} = \frac{v^2 e \tau}{2 \pi \hbar^2} \times \frac{\pi^2 (k_B T)^2}{3}, \quad L_{xx}^{22} = L_{yy}^{22} = \frac{v^2 \tau}{2 \pi \hbar^2} \times \frac{\mu \pi^2 k_B^2 T}{3}. \quad (\text{A6})$$

¹ A. H. Castro Neto, F. Guinea, N. M. R. Peres, K. S. Novoselov, and A. K. Geim, *Rev. Mod. Phys.* **81**, 109 (2009).

² J. G. Checkelsky and N. P. Ong, *Phys. Rev. B* **80**, 081413 (2009).

³ E. H. Hwang, E. Rossi, and S. Das Sarma, *Phys. Rev. B* **80**, 235415 (2009).

⁴ Y. M. Zuev, W. Chang, and P. Kim, *Phys. Rev. Lett.* **102**, 096807 (2009).

⁵ L. Zhu, R. Ma, L. Sheng, M. Liu, and D.-N. Sheng, *Phys.*

Rev. Lett. **104**, 076804 (2010).

⁶ D. L. Bergman and V. Oganessian, *Phys. Rev. Lett.* **104**, 066601 (2010).

⁷ C. Zhang, S. Tewari, and S. Das Sarma, *Phys. Rev. B* **79**, 245424 (2009).

⁸ I. A. Luk'yanchuk, A. A. Varlamov, and A. V. Kavokin, *Phys. Rev. Lett.* **107**, 016601 (2011).

⁹ P. Wei, W. Bao, Y. Pu, C. N. Lau, and J. Shi, *Phys. Rev. Lett.* **102**, 166808 (2009).

¹⁰ G. Sharma, P. Goswami, and S. Tewari, *Phys. Rev. B* **93**,

- 035116 (2016).
- ¹¹ G. Sharma, C. Moore, S. Saha, and S. Tewari, *Phys. Rev. B* **96**, 195119 (2017).
 - ¹² R. Lundgren, P. Laurell, and G. A. Fiete, *Phys. Rev. B* **90**, 165115 (2014).
 - ¹³ Q. Chen and G. A. Fiete, *Phys. Rev. B* **93**, 155125 (2016).
 - ¹⁴ G. Sharma, P. Goswami, and S. Tewari, *Phys. Rev. B* **96**, 045112 (2017).
 - ¹⁵ T. Liang, J. Lin, Q. Gibson, T. Gao, M. Hirschberger, M. Liu, R. J. Cava, and N. P. Ong, *Phys. Rev. Lett.* **118**, 136601 (2017).
 - ¹⁶ M. N. Chernodub, A. Cortijo, and M. A. H. Vozmediano, *Phys. Rev. Lett.* **120**, 206601 (2018).
 - ¹⁷ B. Skinner and L. Fu, *Science Advances* **4**, 2621 (2018).
 - ¹⁸ B. Sbierski, G. Pohl, E. J. Bergholtz, and P. W. Brouwer, *Phys. Rev. Lett.* **113**, 026602 (2014).
 - ¹⁹ Z. Huang, D. P. Arovas, and A. V. Balatsky, *New Journal of Physics* **15**, 123019 (2013).
 - ²⁰ Y. Ominato and M. Koshino, *Phys. Rev. B* **89**, 054202 (2014).
 - ²¹ P. Hosur, S. A. Parameswaran, and A. Vishwanath, *Phys. Rev. Lett.* **108**, 046602 (2012).
 - ²² K. Landsteiner, *Phys. Rev. B* **89**, 075124 (2014).
 - ²³ B. Fauqué, N. P. Butch, P. Syers, J. Paglione, S. Wiedmann, A. Collaudin, B. Grena, U. Zeitler, and K. Behnia, *Phys. Rev. B* **87**, 035133 (2013).
 - ²⁴ D. Xiao, Y. Yao, Z. Fang, and Q. Niu, *Phys. Rev. Lett.* **97**, 026603 (2006).
 - ²⁵ T. Liang, J. Lin, Q. Gibson, T. Gao, M. Hirschberger, M. Liu, R. J. Cava, and N. P. Ong, *Phys. Rev. Lett.* **118**, 136601 (2017).
 - ²⁶ Z. Zhu, X. Lin, J. Liu, B. Fauqué, Q. Tao, C. Yang, Y. Shi, and K. Behnia, *Phys. Rev. Lett.* **114**, 176601 (2015).
 - ²⁷ Y. Ferreira, A. A. Zyuzin, and J. H. Bardarson, *Phys. Rev. B* **96**, 115202 (2017).
 - ²⁸ E. V. Gorbar, V. A. Miransky, I. A. Shovkovy, and P. O. Sukhachov, *Phys. Rev. B* **96**, 155138 (2017).
 - ²⁹ T. M. McCormick, R. C. McKay, and N. Trivedi, *Phys. Rev. B* **96**, 235116 (2017).
 - ³⁰ V. Pardo and W. E. Pickett, *Phys. Rev. Lett.* **102**, 166803 (2009).
 - ³¹ V. Pardo and W. E. Pickett, *Phys. Rev. B* **81**, 035111 (2010).
 - ³² S. Banerjee, R. R. P. Singh, V. Pardo, and W. E. Pickett, *Phys. Rev. Lett.* **103**, 016402 (2009).
 - ³³ A. Kobayashi, Y. Suzumura, F. Piéchon, and G. Montambaux, *Phys. Rev. B* **84**, 075450 (2011).
 - ³⁴ Y. Suzumura, T. Morinari, and F. Pichon, *Journal of the Physical Society of Japan* **82**, 023708 (2013).
 - ³⁵ Y. Hasegawa, R. Konno, H. Nakano, and M. Kohmoto, *Phys. Rev. B* **74**, 033413 (2006).
 - ³⁶ P. Adroguer, D. Carpentier, G. Montambaux, and E. Orignac, *Phys. Rev. B* **93**, 125113 (2016).
 - ³⁷ G. Montambaux, F. Piéchon, J.-N. Fuchs, and M. O. Goerbig, *Phys. Rev. B* **80**, 153412 (2009).
 - ³⁸ G. Montambaux, F. Piéchon, J.-N. Fuchs, and M. O. Goerbig, *The European Physical Journal B* **72**, 509 (2009).
 - ³⁹ P. Dietl, F. Piéchon, and G. Montambaux, *Phys. Rev. Lett.* **100**, 236405 (2008).
 - ⁴⁰ G. Y. Cho and E.-G. Moon, *Scientific Reports* **6**, 19198 (2016).
 - ⁴¹ N. Ashcroft and N. Mermin, *Solid State Physics* (Cengage Learning, 2011).
 - ⁴² S. Park, S. Woo, E. J. Mele, and H. Min, *Phys. Rev. B* **95**, 161113 (2017).
 - ⁴³ R. Fletcher, *Semiconductor Science and Technology* **14**, R1 (1999).
 - ⁴⁴ K. Sun, H. Yao, E. Fradkin, and S. A. Kivelson, *Phys. Rev. Lett.* **103**, 046811 (2009).
 - ⁴⁵ I. Mandal and S. Gemsheim, *Condensed Matter Physics* **22**, 13701 (2019), arXiv:1808.03560 [cond-mat.str-el].
 - ⁴⁶ R. M. Nandkishore and S. A. Parameswaran, *Phys. Rev. B* **95**, 205106 (2017).
 - ⁴⁷ I. Mandal and R. M. Nandkishore, *Phys. Rev. B* **97**, 125121 (2018).
 - ⁴⁸ I. Mandal, *Annals of Physics* **392**, 179 (2018).